DISPLACEMENT EFFECT ON MINIMUM DRAG OF A TORPEDO-SHAPED UNDERWATER VEHICLE

Buğra Uğur Yazıcı, Istanbul Technical University, bugur.yazici@gmail.com

ABSTRACT

Autonomous underwater vehicles (AUVs) have gained significant importance across various industrial sectors due to the rapid advancements in technology. These versatile vehicles are crucial assets for many industrial companies, as they enable the execution of challenging missions. To enhance the operational capabilities of AUVs while accommodating different speeds and configurations, it becomes imperative to optimize their profiles. This study investigates the impact of two distinct velocity profiles on the optimal hull shape of a torpedo-shaped underwater vehicle.

During the optimization phase, two different approaches are employed. The first approach considers the displacement, length, and beam of the AUV's hull shape as constraints during the variant creation phase. In contrast, the second approach incorporates the same constraints but excludes the displacement factor. A comparative analysis is conducted to assess the obtained results and evaluate the influence of the two velocity profiles: one corresponding to the operational speed and the other to the maximum speed of the vessel.

KEYWORDS

Autonomous Underwater Vehicle, Computational Fluid Dynamics, Resistance, Shape Optimization

1. INTRODUCTION

Autonomous Underwater Vehicles (AUVs) represent unmanned and wireless/untethered platforms, extensively employed for underwater scientific research, seabed mapping, pipe and submarine system surveillance, bathymetric scanning, and specialized military tasks. Notably, AUVs operate independently, devoid of physical connections to shore-based cables or service vehicles, and conduct pre-defined missions through operator or controller programming. To enable fully autonomous operations, AUVs are equipped with onboard energy, which partially drives the propeller and propulsion systems. Consequently, the design of AUVs assumes critical significance in determining the hull shapes, considering the aforementioned design limitations.

Previous studies have extensively explored the design aspects of naval submarine shapes with a focus on hydrodynamics, as evident in Joubert's works from 2004 and 2006. Additionally, Khalizev and Kormilitsin (2001) provided a comprehensive evaluation of submarine exterior hull shape selection, encompassing considerations like general arrangement, hydrodynamics, dynamic stability, flow noise, and sonar efficiency. Hydrodynamic design materials for naval submarine hull forms and appendages were also contributed by Moonesun in 2013. The combination of AUV resistance estimation and shape optimization has been a subject of significant research. Parsons, Goodson, and Goldschmied (1974) presented an algorithm for the optimization of axisymmetric bodies in a finite constrained parameter space, using eight parameters and numerical drag calculation methods based on various flow phenomena. Myring (1976) introduced a viscous-inviscid interaction method to predict axisymmetric body drag by dividing the solution domain into potential flow and viscous boundary layers, offering drag comparison for modified tail and nose shapes. Schweyher, Lutz, and Wagner (1996) implemented an evolutionary optimization algorithm for obtaining minimum-drag axisymmetric

bodies. Lutz and Wagner (1997) developed a source distribution model for modeling body contour, using it as design variables to minimize drag within predefined design space. Alvarez, Bertram, and Gualdesi (2009) investigated optimal hull shapes of underwater vehicles near free surfaces using a first-order Rankine panel method to reduce wave resistance. Gao (2016) performed hull shape optimization using particle swarm optimization and multi-island genetic algorithms, validating the results with experimental data. Alkan (2013) proposed a hydrodynamic optimization method employing Response Surface Methodology (RSM) from Computational Fluid Dynamics (CFD) data to minimize AUV hull resistance. Tian (2017) presented a method to optimize the formation of a leader-follower relationship in an AUV fleet, aiming to minimize overall resistance. Joung (2012) introduced a Design of Experiment (DOE) methodology to reduce the drag force of a conceptual AUV hull and its ducted propeller. Moreover, Yazici and Bal (2021) conducted an investigation on the impact of different bow forms in terms of drag and other characteristics, and further performed an optimization study on the bow form of an AUV using Bezier curves for parametrization.

In this research, CFD data was utilized to establish the correlation between velocity and displacement on the resistance characteristics for a torpedo shape AUV. The primary objective was to minimize the total drag of the Myring hull design. The process commenced by creating a parametric representation of the Myring curves utilizing SALOME-CAD software. Subsequently, an AUV hull known as REMUS, as detailed in Prestero's work (1994), was generated and subjected to computational analysis using the open source CFD software, OpenFOAM. To validate the obtained results, a mesh dependency study was conducted and compared with experimental data. The study further encompassed optimization investigations with varying speed and constraint configurations to determine the optimal hull form within the designated design space. For this purpose, a genetic algorithm was employed to achieve the desired optimum shapes.

2. THEORETICAL BACKGROUND AND NUMERICAL METHOD

2.1 GEOMETRIC DEFINITIONS

For the parameterization of AUV hull shapes, a Myring-type body was employed. This body type comprises a nose and a tail section, linked by a middle cylindrical segment. The nose is characterized by a modified semi-elliptical radius distribution, as shown below:

$$r(x) = \frac{1}{2}d\left[1 - \frac{x-a^2}{a}\right]^{\frac{1}{n}} \qquad (1)$$

The axial distance to the nose tip is denoted by "x," with "a" representing the length of the nose section, "d" indicating the middle hull diameter, and "n" signifying the index of the nose shape. Larger values of "n" result in a more substantial and plumper body of revolution. The middle cylindrical section is described as follows:

$$r(x) = \frac{1}{2}d \qquad (2)$$

and the tail is defined by a cubic relationship as:

$$r(x) = \frac{1}{2}d - \left(\frac{3d}{2c^2} - \frac{\tan\theta}{c}\right)(x-a-b)^2 + \left(\frac{d}{c^3} - \frac{\tan\theta}{c^2}\right)(x-a-b)^3 \qquad (3)$$

Here, b and c are the lengths of the middle and tail sections, respectively. θ is the tail semi-angle. Figure 1 shows a schematic view of the Myring-type body.

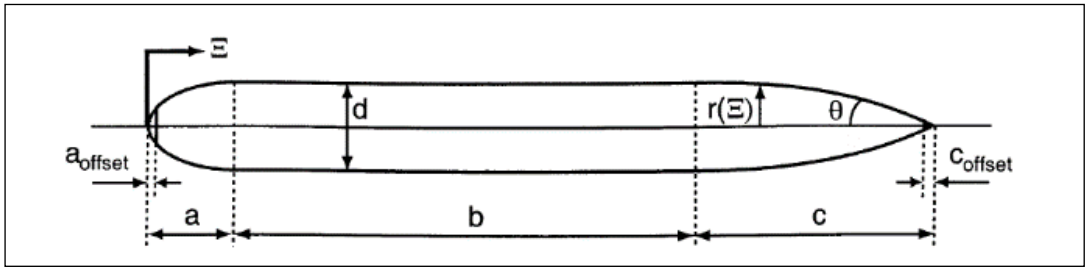

Figure 1: Myring Profile

2.2 NUMERICAL METHOD AND FLOW SOLVER

The drag analyses of the AUV were conducted using the advanced open-source Computational Fluid Dynamics (CFD) code, OpenFOAM, which solves the Reynolds-Averaged Navier-Stokes (RANS) equations. To simulate the turbulent flow around the AUV, the k−omega Shear Stress Transport (k−ω SST) turbulence model proposed by Menter et al. (2003) was employed. The momentum and turbulence terms were treated using a second-order upwind scheme, while the velocity-pressure interaction was managed through the SIMPLE algorithm. The governing equations considered for this steady-state, three-dimensional, incompressible flow analysis included the continuity and momentum equations.

$$\frac{\partial u_i}{\partial x_i} = 0 \qquad (4)$$

is the continuity and,

$$\rho\overline{u_j}\frac{\partial \overline{u_i}}{\partial x_j} = \rho\overline{f_i} + \frac{\partial}{\partial x_j}\left[-\bar{p}\delta_{ij} + \mu\left(\frac{\partial \overline{u_i}}{\partial x_j} + \frac{\partial \overline{u_j}}{\partial x_i}\right) - \rho\overline{u_i' u_j'}\right] \qquad (5)$$

is the momentum equation where x_i and v_i express the tensor form of axial coordinates and velocities, respectively. δij is the Kronecker Delta, ρ is the density of fluid, ν is the kinematic viscosity of fluid and $\rho\overline{u_i' u_j'}$ are the unknown Reynolds stresses. For the turbulence modelling, k−ω turbulence is used to simulate the turbulent flows. Further details about the k−ω turbulence model can be found in Wilcox (2006). SimpleFoam of OpenFOAM v2212 (ESI OpenCFD, 2022) which is a steady-state solver for incompressible, turbulent flows and employs the SIMPLE algorithm is used to solve Eqs.4-5.

2.3 INITIAL GEOMETRY AND BOUNDARY CONDITIONS

Table 1 presents the main particulars of the initial AUV geometry, referred to as Remus. The dimensions of the computational domain are illustrated in Fig. 2, while Fig. 3 depicts the boundary conditions applied to the domain. The left and right sides of the computational domain are specified as the velocity inlet and pressure outlet, respectively. The Myring hull is designated as a no-slip wall to enforce the kinematic boundary condition. Additionally, the surrounding surfaces are defined as a symmetry plane.

Table 1: Main Particulars of Initial Hull Form (Remus)

Parameter	Value	Units	Description
a	1.91e-001	m	Nose Length
a_{offset}	1.65e-002	m	Nose Offset

b	6.54e-002	m	Midbody Length
c	5.41e-001	m	Tail Length
c_{offset}	3.68e-002	m	Tail Offset
n	2.00	n/a	Exponential Coefficient
θ	4.36e-001	radians	Included Tail Angle
d	1.91e-001	m	Maximum Hull Diameter
l_f	8.28e-001	m	Vehicle Forward Length
l	1.33e+000	m	Vehicle Total Length

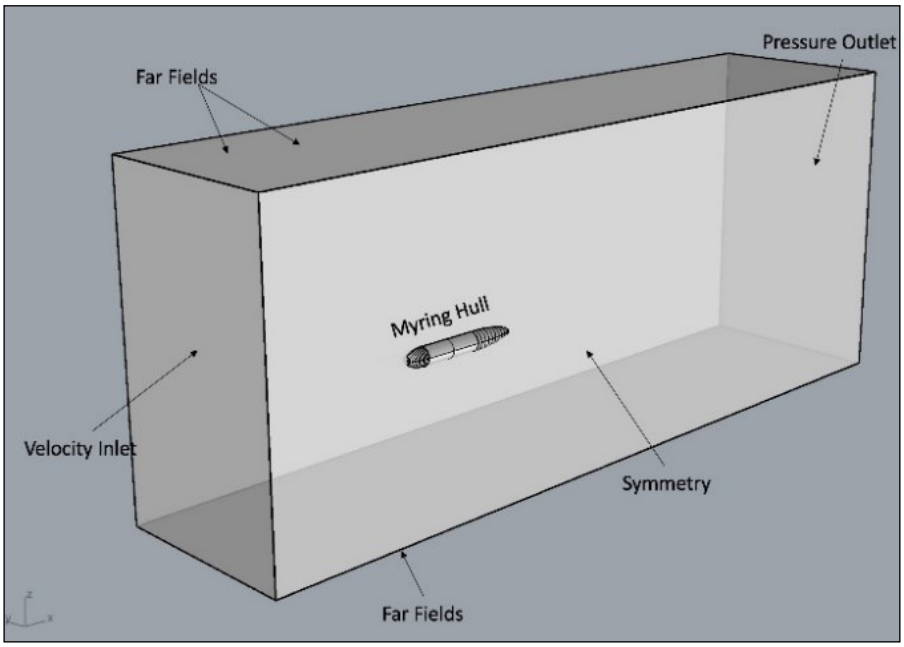

Figure 2: Boundary Conditions

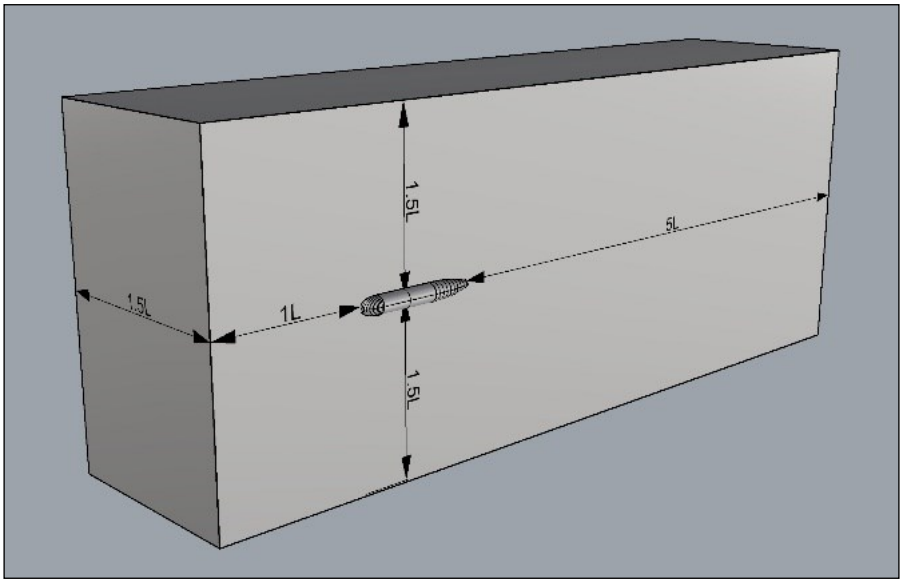

Figure 3: Computational Domain Size

2.4 GRID GENERATION

For the drag analyses, unstructured hexahedral elements have been generated to encompass the hull using the OpenFOAM extension cfMesh. The grid generation process employed the Cartesian mesh algorithm, resulting in a fully hexahedral mesh structure. Fig. 4 illustrates the unstructured mesh surrounding the Myring hull. To maintain acceptable wall y+ values, the mesh size on the hull surface was adjusted. Specifically, the average wall y+ value of the submarine hull was kept below 1, ensuring an accurate representation of the boundary layer for both 0.5144 m/s and 1.54 m/s inlet velocities.

2.5 GRID GENERATION

A mesh dependency study was conducted, employing unstructured meshes of varying sizes. The obtained results were then compared with experimental data. According to Prestero's findings in 1994, the total drag of the Myring hull alone at a flow velocity of 1.5 m/s was measured to be 3.39N through towing tank experiments for a double hull configuration. Since the analyses were conducted for only half of the hull, the actual drag force was considered half of the experimental value, resulting in a value of 1.695N, as presented in Table 2.

Table 2: Mesh Dependency Study

Mesh Size	Cell Number	Total Drag [N]	Error %
Coarse	187k	1.8445	8.88
Medium	677k	1.7797	4.76
Fine	993k	1.7207	1.68

The uncertainty assessment was performed using the GCI method. Four different mesh size within the spatial discretization was employed and numerical uncertainties were calculated as recommended in several studies and guidelines (Celik et al. 2008, ITTC 2008).

Table 3: Verification Study

Parameter	Value
N_1	187k
N_2	677k
N_3	993k
φ_1	1.8445
φ_2	1.7797
φ_3	1.7207
GCI_{medium}	%0.8
GCI_{fine}	%5.5
R	0.91

According to verification study given in Table 3, spatial mesh discretization has monothonic convergence since R value is between zero and one. N denotes number of cells in the mesh for each case and φ denotes scalar value which is the total drag in this case. The most convenient mesh size for the optimization is Fine mesh with 993k cells. General outlook of the fine mesh is shown in Fig. 5.

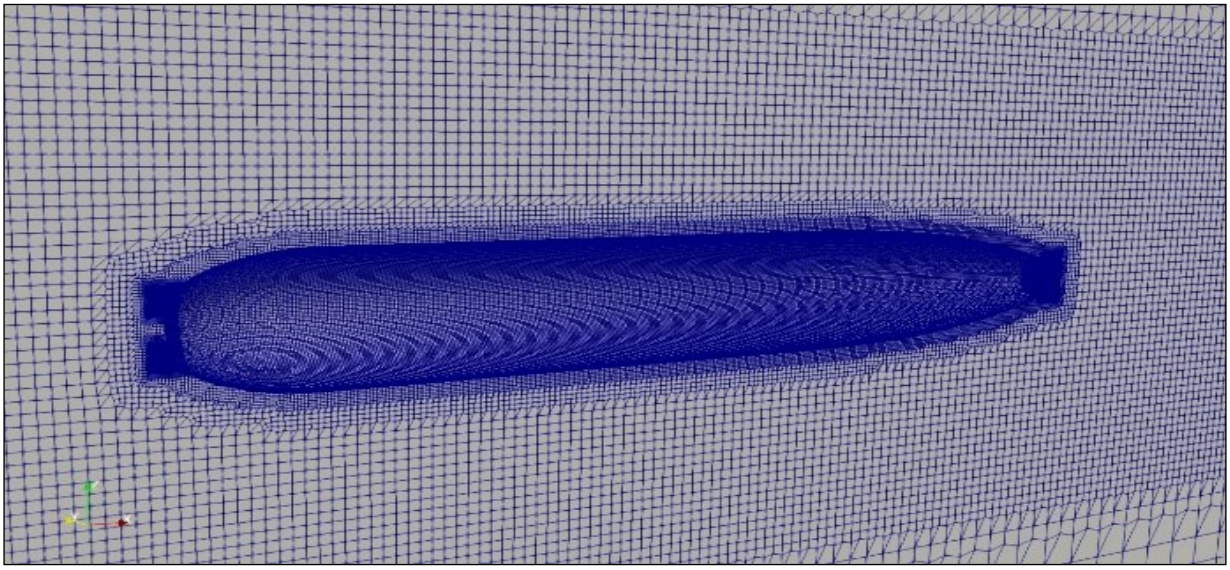

Figure 4: Unstructured Mesh Around Hull

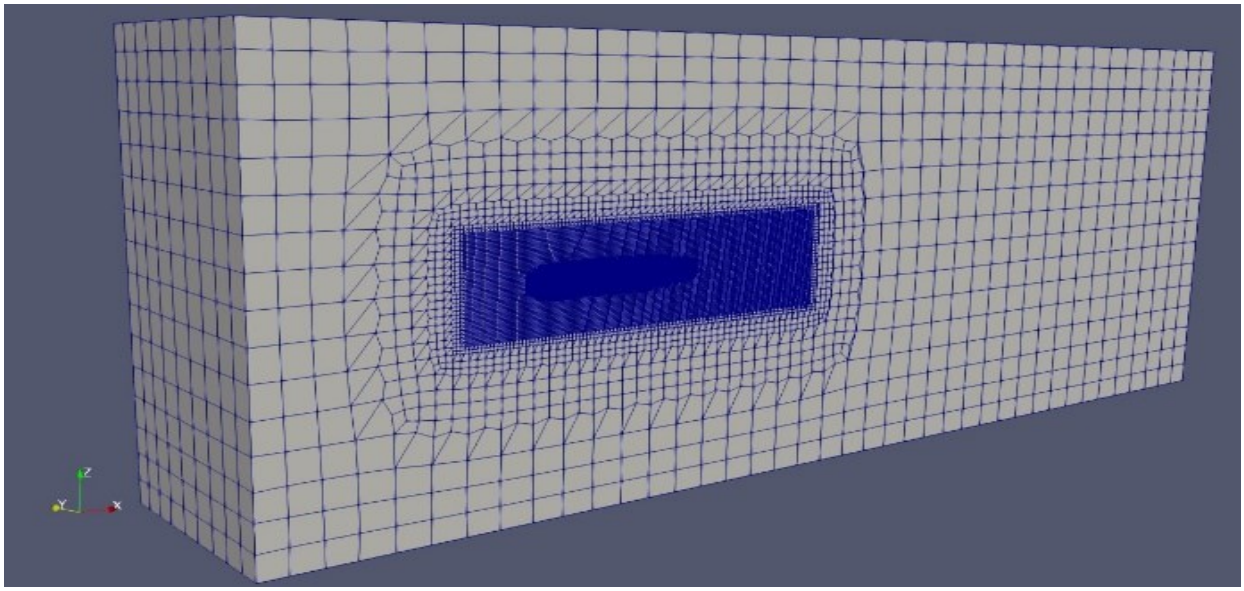

Figure 5: General Outlook of the Fine Mesh

3. OPTIMIZATION

The genetic algorithm details have been previously presented in Yazici and Bal's work (2021). For the optimization process, the open-source DEAP library (Fortin, 2012) was utilized. To ensure the meaningfulness of variant parameters, bitwise mutation was disabled when creating an instance of the genetic algorithm. Crossover and mutation probabilities were set to 1.0. It was observed that setting these parameters relatively low led to the creation of similar variants in the populations, resulting in a decline in overall performance of the optimization process and an increase in total computational time.

The optimization process comprised 10 generations, each consisting of 15 individuals (variants) within the population. Two separate optimization processes were conducted. The first aimed to assess how the length and diameter of the hull shape impacted the overall drag. This optimization process was designed to verify the functionality of the developed algorithm. Subsequently, the length and

diameter of the hull shape were held constant, while the other five parameters, namely a, b, c, n, and θ, were modified.

The optimization parameters and limits for the current section are provided in Table 4. It should be noted that the design parameters are generated as per Myring's contour definition. Myring (1976) assumes a total body length of 100 units, and classifies body types by a code of the form a/b/n/θ/d, where θ is given in radians. REMUS is based on the Myring B hull contour, which is given by the code 15/55/1.25/0.4363/5. "l" which was equal to 100 units. To calculate the nondimensional value of "c," the following equation can be employed:

$$c = l - a - b \qquad (6)$$

Table 4: Design Parameters for Optimization

Parameter	Lower Bound	Upper Bound
a	5	30
b	5	60
n	0.6	3
θ	5	25

The research includes three distinct case studies, each with its findings presented in the subsequent sections. Throughout all case studies, the length and diameter of the hull shapes were maintained at constant values of 1.33 meters and 0.191 meters, respectively. The term "V_{inlet}" refers to the inlet velocity, while the function "f" returns the total drag for each variant generated within the optimization loop. Additionally, "Disp" represents the displacement of the individuals.

3.1 CASE STUDY – 1

For this optimization problem, object function and the constraints are defined as follows:

Minimize :

$f(\text{Remus}(a, b, n, \theta, l, d), V_{inlet})$

Subject to :

$5 \leq a \leq 30$
$5 \leq b \leq 60$
$0.6 \leq n \leq 3$
$5 \leq \theta \leq 25$
$l = 100$
$d = 5$
$V_{inlet} = 1.54$ m/s

The total drag force of the optimized hull form was determined to be 1.3652 N. In contrast, the initial drag of the original Remus, with both a_{offset} and c_{offset} set to zero, amounted to 1.67826 N. This indicates that the total drag of the initial form has been reduced by 18.4%. Table 5 presents the corresponding normalized (nondimensional) values and their corresponding actual values.

However, it is essential to acknowledge that the initial and optimum forms possess different volumes. Specifically, the initial form has a volume of 0.0303 m3, whereas the optimum form has a volume of 0.02095 m3. Consequently, the optimum form boasts a 30.1% lower volume compared to the initial one. The best variant from the case study and the initial geometry are shown in Fig. 6.

Table 5: Parameters for Best Variant

Parameter	Myring Constants	Dimensions
a	28.984	0.3854872 [m]
b	10.816	0.1438528 [m]
c	50.200	0.66766 [m]
d	25	0.190988 [m]
n	1.6502	1.6502
θ	0.0999[radians]	5.72443 [degrees]
l	100	1.33 [m]
Displacement	0.02095 [m^3]	

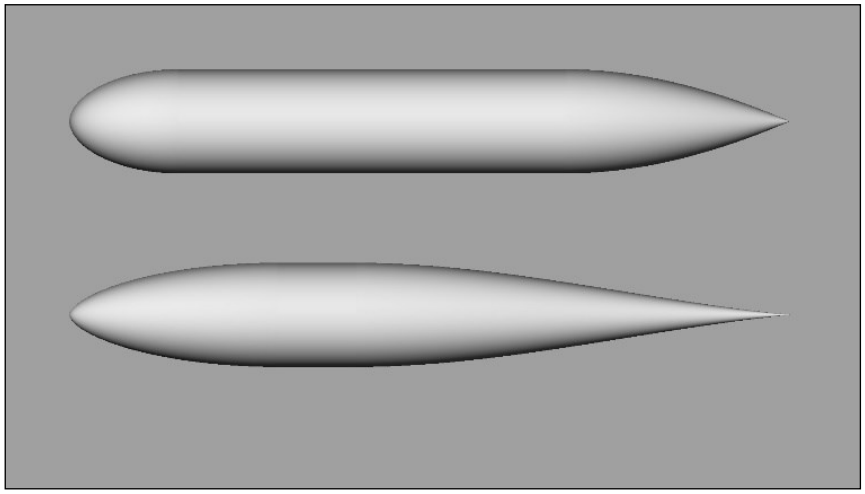

Figure 6: Initial Hull (above) and Optimized Hull (below) for Case Study-1

In Fig.8a, Fig.8b and Fig.9, the pressure and velocity distributions respectively are shown as compared with each other (the initial hull and the optimized hull). It can be noted that the negative pressure contours have abrupt change along the length of the initial hull as compared with the optimized hull. Pressure distribution on the nose section of the initial hull is changing rapidly. However, the optimized hull has more smooth transition and pressure does not drop significantly in the nose section. It has the same trend when comparing the velocities on the forms. Stagnation contours in the foremost of the initial hull is bigger than those of optimized hull. It can be observed that the velocities that are equal to inlet velocity reached out for the optimized hull on its middle section more than initial form.

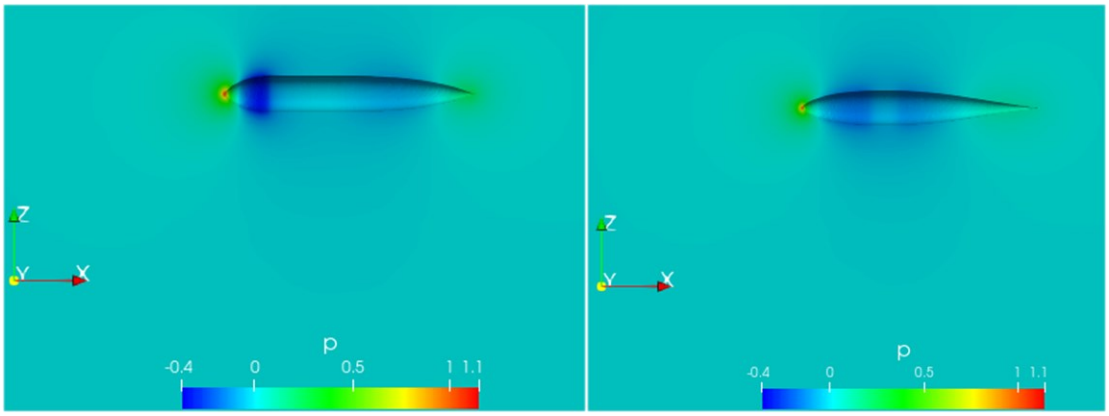

Figure 7a: Pressure Distribution on Initial Hull (left) and Optimized Hull (right)

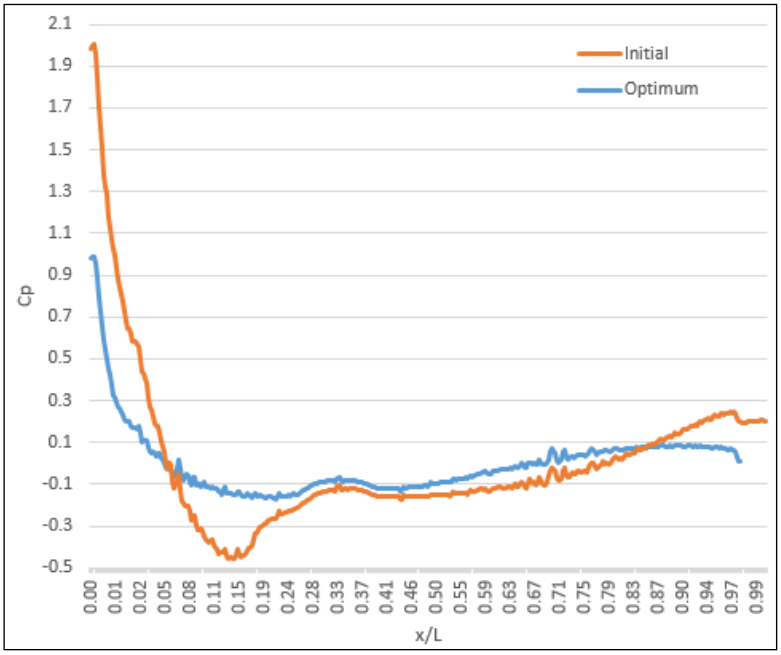

Figure 7b: Cp Distribution on Initial Hull (red) and Optimized Hull (blue)

In Fig. 10, Q-Criterion with vorticity contour is shown. Vorticities are dramatically reduced in nose and tail sections of the optimum hull as compared to the initial hull.

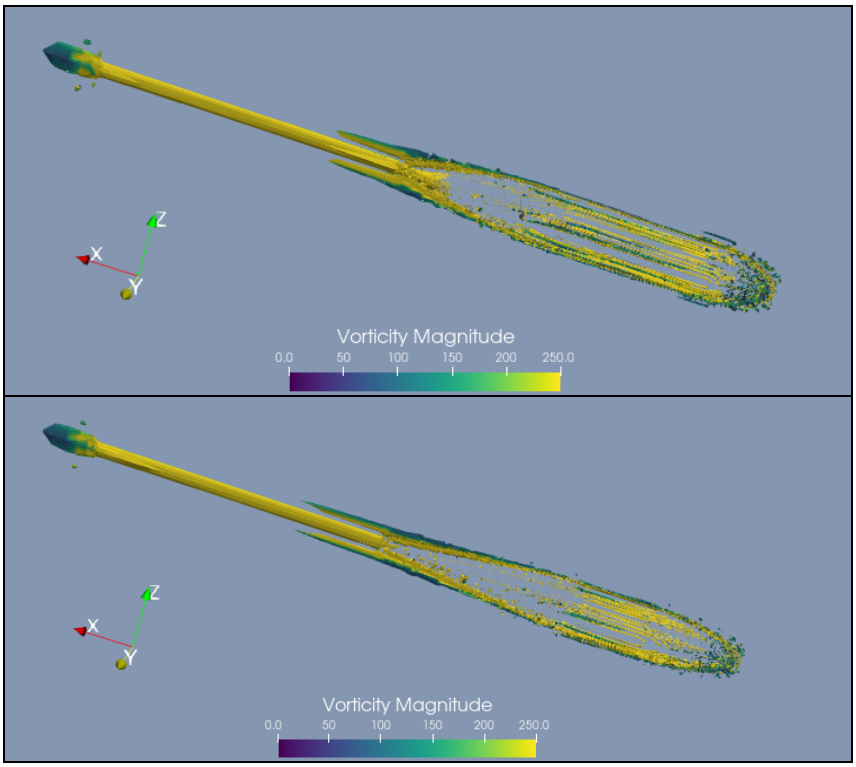

Figure 8: Q-Criterion (value = 1000) with Vorticity Contour.
Initial Hull (left) and Optimized Hull (right)

3.2 CASE STUDY – 2

For this optimization problem, displacement is fed as a constraint in the optimization loop in order to see the effect of the displacement on the resistance characteristics. Object function and the constraints are defined as follows:

Minimize :

$f(\text{Remus}(a, b, n, \theta, l, d), V_{inlet}, \text{Disp})$

Subject to:

$5 \leq a \leq 30$
$5 \leq b \leq 60$
$0.6 \leq n \leq 3$
$5 \leq \theta \leq 25$
$l = 100$
$d = 5$
$V_{inlet} = 1.54$ m/s
$0.90 * \text{Disp\_initial} < \text{Disp} < 1.10 * \text{Disp\_initial}$

The total drag force of the optimized hull form was determined to be 1.5719 N. As indicated in the Case Study-1, the initial drag of the original Remus amounted to 1.67826 N. This indicates that the total drag of the initial form has been reduced by 6.337%. Table 6 presents the corresponding normalized (nondimensional) values and their corresponding actual values. Number of cells of the optimized design is 789k.

Table 6: Parameters for Best Variant

Parameter	Myring Constants	Dimensions
a	21.792481	0.224419 [m]
b	8.132331	0.580304 [m]
c	37.744361	0.525277 [m]
d	0.191	0.191 [m]
n	1.0364	1.0364
θ	0.408227 [deg]	23.389662 [deg]
l	100	1.33 [m]
Displacement	0.028719 [m^3]	

It should be noted that the volume difference between the initial and optimum forms is 9.48%. The best variant from this case study and the initial geometry are shown in Figure 9.

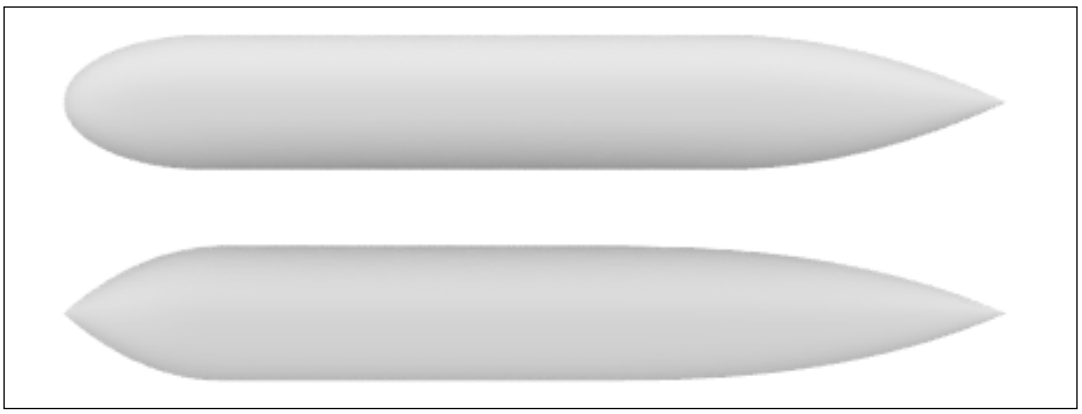

Figure 9: Initial Hull (above) and Optimized Hull (below) for Case Study-2

3.3 CASE STUDY – 3

For this optimization problem, displacement is also fed as a constraint in the optimization loop, as done in Case Study-2. The difference between Case Study-2 and Case Study-3 lies in the inlet velocities. The objective function and constraints are defined as follows:

Minimize :

$f(\text{Remus}(a, b, n, \theta, l, d), V_{inlet}, \text{Disp})$

Subject to:

$5 \leq a \leq 30$
$5 \leq b \leq 60$
$0.6 \leq n \leq 3$
$5 \leq \theta \leq 25$
$l = 100$
$d = 5$
$V_{inlet} = 0.5144$ m/s
$0.90 * \text{Disp\_initial} < \text{Disp} < 1.10 * \text{Disp\_initial}$

The total drag force of the optimized hull form was determined to be 0.21133 N. The total drag of the initial form of the original Remus amounted to 0.2267 N at an inlet velocity of 0.5144 m/s. This indicates a reduction of 6.76% in the total drag of the initial form. Table 7 presents the corresponding normalized (nondimensional) values and their corresponding actual values. Number of cells of the optimized design is 819k.

Table 7: Parameters for Best Variant

Parameter	Myring Constants	Dimensions
a	18.07996	0.240463 [m]
b	18.905549	0.251444 [m]
c	63.014491	0.838093 [m]
d	25	0.191 [m]
n	1.410261673	1.410261673
θ	0.397815 [deg]	22.793102 [deg]
l	100	1.33 [m]
Displacement	0.02884944 [m3]	

It should be noted that volume difference between initial and optimum forms is 9.53%. The best variant from this case study and the initial geometry are shown in Fig. 10.

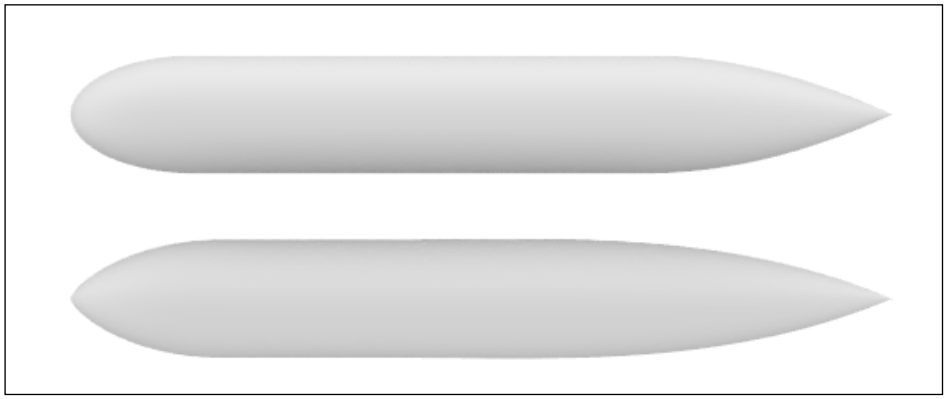

Figure 10: Initial Hull (above) and Optimized Hull (below) for Case Study-3

4. CONCLUSIONS

The total drag force of a well-known axisymmetric AUV geometry based on REMUS is minimized through an optimization study that utilizes sensitivity analysis and genetic algorithms. The study makes use of various open-source software and libraries, including SALOME-CAD for parametric geometry development, cfMesh for unstructured meshing, OpenFOAM for CFD calculations, and DEAP for genetic algorithms. In summary, the key points of the study are as follows:

- The utilization of genetic algorithms has enabled the discovery of an optimal hull shape for different configurations of an AUV. The bitwise mutation method within the algorithm has been eliminated to restrict the design variables of newly generated hull forms, resulting in a consistent and robust design space.
- During the optimization phase of Case Study-1, the genetic algorithm successfully identified the optimum hull shape in the fifth generation, each comprising 15 variants. The best individuals among the generations coincided with the streamlined shape recommended by Vishwakarma (2012). By keeping the total length and maximum hull diameter constant as "Myring B Hull Contour - REMUS," a 18.4% reduction in drag was achieved through the genetic algorithm. The optimal AUV form exhibited a significant change in displacement, amounting to a 30% difference.
- To address the abrupt displacement change observed during the optimization phase, displacement was introduced as a constraint in the optimization problem for Case Study 2 and 3.
- Both Case 2 and 3 achieved reductions of up to 7% in their respective forms. The optimization algorithm consistently aimed to minimize displacement within the feasible range, demonstrating the effectiveness of the optimization setup.
- Each simulation required approximately 11.5 minutes to compute using an Intel® i7-12800HX Processor (25M Cache, 4.8 GHz / 16 parallel cores and 24 threads).
- The primary distinction between the optimal geometries of Case Study-2 and Case Study-3 lies in the shorter parallel midbody length of Case Study-3 compared to Case Study-2. Additionally, the forebody of Case Study-2 exhibited more pronounced curvature compared to Case Study-3. The disparities between the initial and optimum forms of Case Study-2 and Case Study-3 are illustrated in Figure 11.

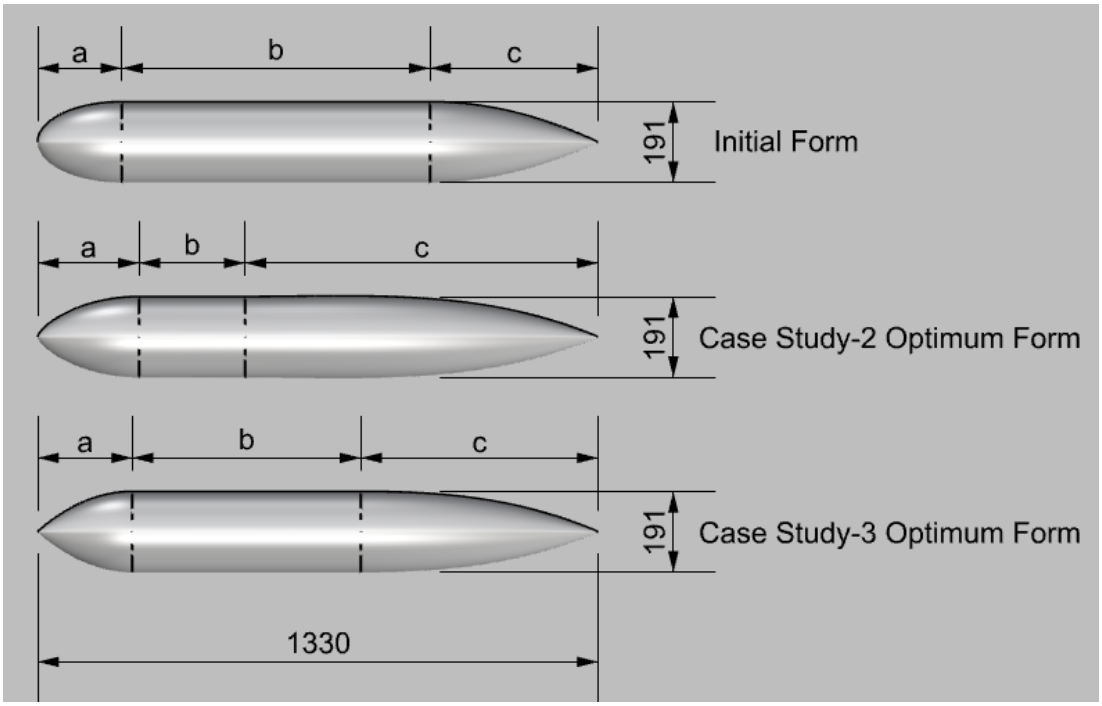

Figure 11: Comparison Between Forms

5. REFERENCES

Alkan B., Isman M.K., (2013). "Hydrodynamic Design Optimization of an Autonomous Underwater Vehicle based on Response Surface Methodology", Conference: 7th International Advanced Technologies Symposium(IATS'13).

Bertram V. Gualdesi L. Alvarez, (2009). "Hull hydrodynamic optimization of autonomous underwater vehicles operating at snorkeling depth." Ocean Engineering, 36(1):105–112.

Celik I.B., Ghia U., Roache, P.J, Freitas C.J., Raad P.E (2008). "Procedure for Estimation and Reporting of Uncertainty Due to Discretization in CFD Applications.", Journal of Fluids engineering, 130(7), 078001. doi:10.1115/1.2960953.

D. F. Myring., (1976) "A theoretical study of body drag in subcritical axisymmetric flow." Aeronautical Quarterly, 27(3):186–194.

David C. Wilcox, (2006). "Turbulence Modeling for CFD." Canada, La, 3 edition.

F-A. Fortin, F-M. De Rainville, M-A. Gardner, M. Parizeau, and C. Gagne, (2012). "DEAP: Evolutionary algorithms made easy." Journal of Machine Learning Research, 13:2171–2175.

ITTC Recommended Procedures and Guidelines. (2008) "Uncertainty Analysis in CFD Verification and Validation Methodology and Procedures.", 7.5-03-0101.

Lutz T. , Wagner S., Schweyher, H., (1996) "An optimization tool for axisymmetric bodies of minimum drag". 2nd International Airship Conference, Stuttgart /Friedrichshafen.

M. Vishwakarma, V. Parashar and V.K.Khare, (2012). "Geometrical characteristics of streamlined shapes. Technical Report 2962," International Journal of Engineering Research and Applications, Vol.2, Issue 6, pp 787-792.

Melanie Mitchell, (1996). "An Introduction to Genetic Algorithms." Cambridge, MA: MIT Press.

Menter F.R., Kuntz M., and Langtry R. (2003). "Ten years of industrial experience with the SST turbulence model." In Proceedings of the fourth international symposium on turbulence, heat and mass transfer, pages 625–632, Antalya, Turkey.

Oleg.A.Khalizev Yuri.N.Kormilitsin, (2001). "Theory of Submarine Design".Saint Petersburg State Maritime Technical University, Russia, pages 185–221.

P.Charmdooz U.M.Korol M.Moonesun, M.Javadi, (2013). "Evaluation of submarine model test in towing tank and comparison with CFD and experimental formulas for fully submerged resistance".Indian Journal of Geo-Marine Science, vol.42(8), pages 1049–1056.

P.N.Joubert, (2004). "Some aspects of submarine design: part 1: Hydrodynamics". Australian Department of Defence.

P.N.Joubert, (2006). "Some aspects of submarine design: part 2: Shape of a Submarine 2026".Australian Department of Defence.

Prestero T., (1994). "Verification of a Six-Degree of Freedom Simulation Model for the REMUS Autonomous Underwater Vehicle". University of California at Davis, pages14–15.

T-H Joung, K. Sammut, F. He, S-K Lee, (2012). “Shape optimization of an autonomous underwater vehicle with a ducted propeller using computational fluid dynamics analysis”, International Journal of Naval Architecture and Ocean Engineering, Volume 4, Issue 1, Pages 44-56.

Ting G., Yaxing W., Yongjie P., and Jian C., (2016). “Hull shape optimization for autonomous underwater vehicles using cfd.” Engineering Applications of Computational Fluid Mechanics, 10(1):599–607.

Wagner S. Lutz, T., (1998). “Drag reduction and shape optimization of airship bodies.” Journal of Aircraft, 35(3):345–351.

Wenlong T., Zhaoyong M., Fuliang Z., Zhicao Z., (2017). "Layout Optimization of Two Autonomous Underwater Vehicles for Drag Reduction with a Combined CFD and Neural Network Method", Complexity, vol. 2017, Article ID 5769794, 15 pages.

Yazici B.U., Bal S., (2021). “Hydrodynamic Optimization of a Submarine Forebody Using Bezier Curve and Genetic Algorithms”, 2nd International Congress On Ship And Marine Technology GMO-SHIPMAR.

Yazici B.U., Bal S., (2021). “Hydrodynamic Comparison of Bow Forms for a Model Submarine”, 4th Global International Conference on Innovation in Marine Technology and Future of Maritime Transportation Conference (GMC’21).